RESEARCH ARTICLE

Adaptive Spatial Complex Fuzzy Inference Systems With Complex Fuzzy Measures

LE TRUONG GIANG[1,2], LE HOANG SON[3], NGUYEN LONG GIANG[4], NGUYEN VAN LUONG[1], LUONG THI HONG LAN[5], TRAN MANH TUAN[5], AND NGUYEN TRUONG THANG[4]

[1]Center of Quality Assurance, Hanoi University of Industry, Hanoi 100000, Vietnam
[2]Graduate University of Science and Technology, Vietnam Academy of Science and Technology, Hanoi 100000, Vietnam
[3]VNU Information Technology Institute, Vietnam National University (VNU), Hanoi 700000, Vietnam
[4]Institute of Information Technology (IoIT), Vietnam Academy of Science and Technology, Hanoi 100000, Vietnam
[5]Faculty of Computer Science and Engineering, Thuyloi University, Hanoi 116705, Vietnam

Corresponding author: Nguyen Truong Thang (ntthang@ioit.ac.vn)

ABSTRACT Fuzzy inference systems, in general, and complex fuzzy inference systems, in particular, play an increasingly important role in many fields, such as change detection, image classification, recognition problems, etc. Despite being the well-known technique to solve with time series data, the rulebase still has the considered limitation because of the directly affecting the results as well as the processing time of these methods. To overcome this limitation, this study proposes an Adaptive spatial complex inference system that can automatically infer and adapt to the new remotely sensed image. In the proposed model, to predict the image of time t + 1, the system will generate a new rulebase according to this expected image. This new rulebase and the previous Co-Spatial-CFIS+ rulebase are evaluated using a complex fuzzy measure. This measure is built by determining the intersection domain between two rule spaces; this intersection value estimates removing, merging, or adding a newly generated rule into the current rulebase. Finally, a more suitable set of rules is obtained for image prediction. To illustrate the efficiency of the proposed approach, it is applied to the remote sensing cloud image data of the U.S. Navy. Our model evaluated the model's effectiveness in comparison to the state-of-the-art along studies in detecting changes in remote sensing cloud images. Moreover, the findings of the experiments revealed that the proposed model could improve the change detection results in terms of R^2, RMSE, time-consuming, and the number of rules.

INDEX TERMS Complex fuzzy inference system, remote sensing images, rule pruning, rule-based system, image change detection.

I. INTRODUCTION

Change detection in remote sensing image (RSI) concerns identifying and analyzing changes in multi-temporal pictures captured at different times. This process takes into account correlations between the temporal lags and the observations in the photos. Timely and accurate change detection is critical for gaining insight into the relationships and interactions between human and natural phenomena, enabling better decision-making. Therefore, different approaches have been

The associate editor coordinating the review of this manuscript and approving it for publication was Qi Zhou.

adopted for change detection in RSI, such as artificial neural networks [1], [2], [3], fuzzy modeling [4], [5], [6], [7], mixed methods [8], [9], [10], [11], etc. These approaches offer the potential to improve the accuracy and robustness of change forecasting, particularly in complex and uncertain environments.

The importance of change detection is to specify the significant change that has occurred over a series of images across a period, which helps in decision-making. However, images are often inherently imprecision due to many factors, including observed phenomena, acquisition process, as well as image processing steps. This may affect imprecision in

the objects to be recognized. Hence, fuzzy logic models are one of the suggestions that many researchers pay attention to in developing in order to be able to model and take into account these imprecision, uncertainty, and ambiguity factors of images at different levels. The fuzzy logic system, in general, or fuzzy inference system (FIS), is attractive because they are interpretable and provide an analyst with a deeper insight into the problem. Generally, a FIS is typically superior to other methods regarding memory usage and inference speed. With the rapid advancement of space science and technology, a large amount of Remote Sensing (RS) data with high spatial-temporal resolution has become available, which brings new challenges in describing RSI. Modeling time series RSI can be particularly challenging due to the dynamic characteristics and uncertainty of the data.

In recent year, the complex fuzzy set (CFS) theory has been introduced and provided a practical expression to address problems involving temporal, vague, and periodic elements [12], [13], [14], [15], [16], [17], [18]. CFS can effectively characterize data by considering an event's amplitude and phase values. Each component of CFS is assigned a complex fuzzy membership function, and the values lie on the unit circle in the complex plane. Inspired by the success of CFS in modeling time series data, CFS-based systems have become increasingly important as a new approach to solving temporal or time series datasets. This approach has shown great promise in addressing the challenges of time series RSI.

Because earlier works have indicated that fuzzy models built using complex fuzzy logic could be very accurate in time-series forecasting, Chen et al. [22] introduced the first neuro-fuzzy system-based CFS for time series forecasting. Then, Yazdanbakhsh et al. presented an extended version of the forward- and backward-pass computations, the Randomly Adaptive Neural Complex Fuzzy Inference System (RANCFIS) [23]. To enhance the first version, the author uses a randomized-learning to train and optimize parameters in CFIS. Moreover, another related performance [24] is suggested to improve computational time and accuracy for the forecasting model. In this work, the author applied the Fast Fourier Transform algorithm is applied to determine the prevailing frequencies in time-series data and then established CFS to match them as the antecedents of a complex fuzzy rule (CFR).

According to the series of research on complex fuzzy systems, in 2019, Selvachandran et al. introduced the Mamdani complex fuzzy inference system (M-CFIS) [17] as a valuable tool for addressing problems with vague and temporal factors. Subsequently, Lan et al. proposed two enhanced versions of M-CFIS [25], [26]. The first version improved the rulebases by leveraging complex fuzzy measurements and granular computing, while the second version decreased the computational time by employing fuzzy knowledge graphs. These advancements demonstrate the effectiveness of the complex fuzzy sets in representing temporal factors in data. However,

limited attention has been given to incorporating spatial elements in studies utilizing CFS.

In recent research, Giang et al. [27] proposed a system for handling spatial-temporal data using a CFIS. This system utilized the FWADAM+ optimization algorithm to optimize the rule parameters. However, when applied to time series image forecasting, the model's effectiveness was reduced by accumulating step-by-step errors over time. Besides, establishing new rules poses a challenge as they may overlap or intersect with existing ones, leading to longer processing times and unexpected errors. The large rule generation time and quality of the rulebase were the main challenge and motivations for our research. However, some obstacles were encountered in the process of tackling the challenges. Firstly, we observed that generating rules for new images was a large time-consuming in previous studies. We made theoretical and practical modifications, such as adjusting the clustering algorithm's number of clusters or replacing the clustering algorithm, but the rest could have been a better story. To address this issue, we adopted methods that directly generate rules from images with significantly faster processing time and minimize errors. Second, with the generating rule evaluators. Initially, determining the intersection of two rules using 3-class integrals for calculation was our planned approach. However, this approach involved complex mathematical concepts, so we had to approximate the calculation method. Although this new method resolved the issue of a calculation error, it marginally increased computation time. Hence, we proposed a method while evaluating coefficients for the rule pooling process.

The purpose of our work is to adjust the rulebase to adapt to the new images to improve the accuracy and computational time of the previous work, Co-Spatial CFIS. The paper proposes an adaptive spatial complex fuzzy inference system called Spatial CFIS++ to overcome the limitations of existing methods [27] for change detection. The key contributions of this work are summarized as follows:

First, an adaptive spatial complex fuzzy inference system model based on complex fuzzy measures is introduced for change detection in the RSI series. The proposed model uses the CFS theory to describe both spatial and temporal characteristics of RSI images.

Second, a method is proposed to generate rules directly from the newly obtained images in the testing set. This method involves several steps: preprocessing, fuzzing, calculating the rule space, and determining the rule parameters.

Third, complex fuzzy measures are introduced to compare two rule systems and improve the effectiveness of the rulebase.

Finally, a comparison experiment is conducted to demonstrate the validity and effectiveness of the proposed model. The evaluation parameters used for comparison include RMSE, R^2, computational time, and the number of rules. Overall, the proposed approach outperforms related studies in these metrics.

The remaining paper is arranged to accomplish the above: **Part II** presents the basic knowledge of CFS, complex fuzzy measures, the gray image extraction method using fuzzy logic, and Co-Spatial complex fuzzy inference systems. **Part III** dedicates an adaptive spatial complex fuzzy inference system using complex fuzzy measures. The proposed model's main idea and detailed steps are described and illustrated by an example. **Part IV** represents the practical experimentation and a comparison with some related methods to confirm the model's efficiency. Finally, **Part V** concludes the paper and suggests possible future developments.

II. RELATED WORKS

RSI change detection involves identifying significant differences between RSIs taken at different times. In recent years, automated CD technology has played a crucial role in developing remote sensing applications, with much attention given to soft computing approaches such as fuzzy logic systems. FIS-based strategies have been assumed to be a reliable solution to various image-processing problems, with different rule-generation mechanisms developed to address these issues.

For instance, Mondal et al. [28] proposed a novel approach to fuzzy rule generation based on image features for segmentation and image extraction. The authors noted that traditional methods often need more noise, leading to imprecise results. By leveraging the FIS's ability to handle uncertain information, they could generate rules directly from input images and use them to partition the image. Experimental results on multiple datasets demonstrate the positive impact of this approach on image processing. In [29], an intelligent approach is presented that utilizes RSI processing and Fuzzy Inference System (FIS) to optimize the orientation of solar PV panels. The model uses the cloud cover index to describe the difference between the viewed and reference images and the block-matching algorithm to evaluate cloudy periods. The FIS then uses these parameters to determine the optimal position of the PV panel.

Senthilselvi et al. [30] proposed a method that combines an adaptive neural network and an adaptive FIS solving image-denoising problems. The work takes advantage of the ability to learn the parameters of Artificial Neural Networks (ANN) combined with generating rules from the image and inference capability of ANFIS to reduce the noise of the picture. Another study applying a FIS for images can be mentioned as the study of Tang et al. [31]. The authors proposed an adaptive approach based on a FIS mechanism to balance and improve the quality of hiding information in images. Compared with algorithms of the same group, experimental results show the outstanding performance of the export model. SziovCá et al. [32] proposed a model that uses FIS to detect colorectal polyps in colonoscopy pictures. The author performs image preprocessing, generates rules from the image, and selects regions that may contain tumor pictures for evaluation. The experiment shows promising initial results and opens up new research opportunities for this problem.

Rules play a crucial role in assessing the accuracy of a rule-based inference system. While rule systems in FIS systems are often generated directly from data, for datasets with dynamic elements and time series data, the old rulebase needs to be adjusted and improved to adapt to new data. Duţu et al. [33] introduced Precise and Fast Fuzzy Modeling based on the Mamdani inference mechanism and a powerful rule optimization method. The approach aims to strike a balance between the accuracy of the obtained rules and the speed required to generate them. The authors evaluated the results obtained under various factors to enhance the study's reliability.

The ANFIS model has been used in various studies to improve the efficiency of different systems. One such study [1] used various membership functions and a mixed learning mechanism to adjust the rule parameters of a geographic information system. The experimental results on land subsidence susceptibility mapping in the Marand plain, northwest Iran, have indicated the remarkable effectiveness of the proposed model with high prediction precisions.

Another study [2] utilized the ANFIS model for semantic segmentation of RSI. The authors also encountered limitations in reference results due to the method that generates the rulebase. To address this, the authors have proposed an ANFIS system that automatically infers the fuzzy rules for pixel classification. The experiment achieved good accuracy in classifying pixels despite the limited features and training images.

From the above analyses, it is clear that the variety of methods to generate rules directly from the image and to optimize those rule systems. While these initial approaches have obtained profitable results in practice, they still have limitations that require further consideration and development. Thus, the generation and optimization of rule systems from images offer several possibilities, yet there is a need for ongoing research in this area.

III. BACKGROUND

First, we review basic definitions used throughout this work, including complex fuzzy sets, complex fuzzy measures, gray Image extraction using fuzzy logic, and Co-Spatial CFIS+.

A. COMPLEX FUZZY SET AND COMPLEX FUZZY MEASURE

1) COMPLEX FUZZY SET

Definition 1 [34]: A mapping $A : U \rightarrow D$ is called a complex fuzzy set on U where U is a fixed universe and D is a set of values on a complex unit disk. For any $x \in U$, the complex fuzzy membership function has the form: $\mu_A(x) = h_A(x) e^{j\omega_A(x)}$

2) COMPLEX FUZZY MEASURE

Definition 2 [35]: Assume A, B, and C be three CFSs in a universe of discourse X with membership degrees of $\mu_A(x) = h_A(x) e^{j\omega_A(x)}$, $\mu_B(x) = h_B(x) e^{j\omega_B(x)}$ and $\mu_C(x) = h_C(x) e^{j\omega_C(x)}$ respectively. A distance of complex

fuzzy sets if a function $h : CFS(X) \times CFS(X) \to [0, 1]$ if it satisfies some conditions as follows:

(i) $h(A, B) \geq 0$, $h(A, B) = 0$ *iff* $A = B$
(ii) $h(A, B) = h(B, A)$
(iii) $h(A, B) \leq h(A, C) + h(C, B)$

B. GRAY IMAGE EXTRACTION METHOD USING FUZZY LOGIC

The process of extracting information directly from the image [42] is built based on information related to how to determine the threshold value and transform the spatial region according to the following steps:

Step 1. Read a noisy image as input

Step 2. Determine the focal area of the image according to different threshold values

Step 3. Extract image features by pixel value and the threshold value for the next use.

Step 4. Build an independent input fuzzy function for the image

Step 5. Generate fuzzy rules from previous results. The fuzzy rule generation process consists of 5 steps:

a. Define the space bounds of Input and Output

b. Create fuzzy rules from input data

c. Mapping threshold values obtained by different threshold value evaluation methods in respective fuzzy spaced. Create an association fuzzy rule base based on this association fuzzy rule.

Step 6. Calculate the approximate value obtained in Step 5

Step 7. Display the resulting image.

C. CO-SPATIAL COMPLEX FUZZY INFERENCE SYSTEM

The Co-Spatial complex fuzzy inference system (Co-Spatial CFIS+) [27] is a developing version of Mamdani-CFIS based on CFS theory. for change detection from satellite images contains some stages as follows:

Stage 1: Data preprocessing. In this stage, the color input images are converted to gray images. After reducing the size of images and calculating the complex fuzzy membership values corresponding to representative pixels of images.

Stage 2: Establish the complex fuzzy rules of each image. Determine the boundary point value of each image and generate the rule that has Mamdani-CFIS's form.

Stage 3: Calculate the parameters using for reference and predict the next image. The parameters contain reference value, rule coefficient, and value of neighborhood points.

Stage 4. Optimize the reference parameters using the FWADAM+ method, so the RMSE value reaches a minimum.

Stage 5: Predict the following image. Using obtain parameters to calculate the norm, the interpolation, the defuzzification, and the adjustment of the amplitude and phase components of the forecasted image for the image.

IV. PROPOSED ADAPTIVE SPATIAL COMPLEX FUZZY INFERENCE SYSTEMS

As discussed in the introduction, Giang et al. [27] utilized the FWADAM+ optimization algorithm to optimize the rule parameters in the Co-Spatial CFIS+. However, when forecasting time series problems, the effectiveness of the forecasting system diminishes as the outdated rule system becomes unsuitable for new data. Therefore, this section introduces the proposed Adaptive Spatial Complex Fuzzy Inference Systems model. Part A presents the critical concepts of the model, followed by a detailed description of the proposed model in Part B. Finally, a numerical example is provided to illustrate each step of the proposed model.

A. MAIN SYSTEM

The primary idea of the proposed model is to improve the rulebase in Co-Spatial CFIS+ in the cases of change detection with time-series RSI. The foremost priority of this work is to decrease the computational time and keep the overall efficiency of the model.

The main steps are summarised: Firstly, input images are executed to preprocess data by converting color images to gray photos and determining the image's amplitude and phase term, respectively. The amplitude and phase terms are transformed into the fuzzy domain using the Gaussian complex fuzzy membership function (GCFMF). Then we create the spatial complex fuzzy rule (Spatial-CFR) from the input images.

Next, the rule pruning stage is executed in the rule space domains based on a complex fuzzy measure. Specifically, subdivide the rule space domain into tiny square blocks. Then, determine the relative positions of these blocks in the rule space to calculate the intersection of the two rules.

After obtaining the comparing value between 2 rule spaces, the process of combining or removing rules is executed based on the predefined threshold values. The duplicate or redundant rules are synthesized to improve the quality of the rule base and obtain the new set of rules. The new rule base consists of the old rule base generated based on Co-spatial CFIS+ and the new rule base established directly from the image. Finally, a new set of rules is obtained that adapts and accommodates the novel image set. The new rule base is used to predict the following RSI with the aim of improving both the accuracy and time of the model.

Details of the steps are modeled as shown in Figure 1.

B. DETAILS OF THE PROPOSED SPATIAL CFIS++ METHOD

- **Step 1. Preprocessing input data**
  Preprocessing is performed to prepare data to be applied in the proposed method. The purpose of this step is to execute the preprocessing data to enhance the contrast of images. Some data preprocessing techniques are used, such as: converting all color images into gray images to minimize the algorithm's complexity, determining the
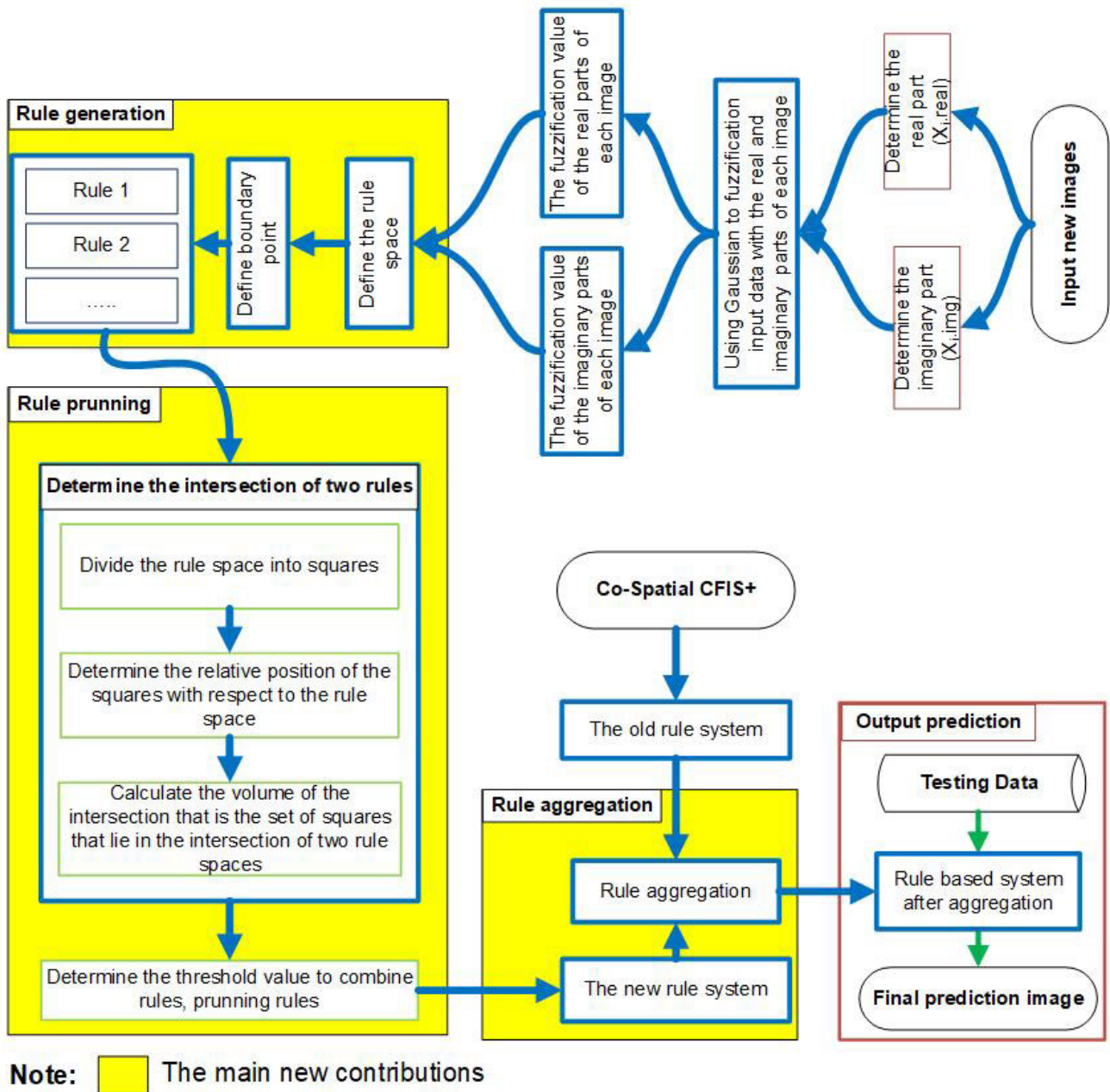
FIGURE 1. The implementation process.

amplitude and phase term of the input image (HoD), and normalizing the data to the form [0,1].

Step 1.1 Convert color images into gray images

All color pixels are displayed as a tint of gray pixels to enhance the contrast of images. This process results in a linear mapping of the color pixel values to the complete range of grays (black to white), creating an image of higher contrast.

Step 1.2 Determine the phase part (HOD)

The phase part is specified by the different points between the first image in the forecast set (the picture has just been obtained) and the last image in the previously

trained. The phase value is obtained using the following formula (1).

$$HoD_i = (I_i - I_{(i-1)}) \tag{1}$$

Step 1.3 Transform the amplitude and phase part of the grayscale image into the form [0,1]

The obtained results received the set of images that have the form: $X(I.HoD)$.

- **Step 2. Fuzzification**

The fuzzification aims to map the image's grey-level intensities from the spatial domain to the fuzzy environment. The two most significant factors of the

membership function are its format and the parameters that express these functions' behavior. The Gaussian complex fuzzy membership function (GCFMF) [36] is used to fuzzify the image. This process's output determines the input data's corresponding complex fuzzy values.

The Gaussian complex fuzzy membership function for the amplitude and phase parts of the image can be calculated as follows:

$$\mu_{gaussian}(x; m, \sigma) = e^{-\frac{1}{2}\left(\frac{x-m}{\sigma}\right)^2} \quad (2)$$

where: σ and m represent the width and center of a complex fuzzy set.

- **Step 3. Determine the rule space**
  After obtaining the parameters from step 2, the process of determining the rule space is executed. The following definition specifies the rule space for satellite images.
  Definition 3: The rule space [35] is the space that is calculated by the formula (3) as follows:

$$\Omega = \{(x, y, z) \,|\, x_{min} \leq x \leq x_{max}, y_{min} \leq y \leq y_{max},$$
$$z_{min} \leq z \leq z_{max}\} \quad (3)$$

  In which:
  - x_{min}: The minimum fuzzy value for amplitude part $Min\left(\mu_{gaussian}(I_i; m_i, \sigma_i)\right)$
  - x_{max}: The maximum fuzzy value for amplitude part $Max\left(\mu_{gaussian}(I_i; m_i, \sigma_i)\right)$
  - y_{min}: The minimum fuzzy value for phase part $Min\left(\mu_{gaussian}(HoD_i; m_i, \sigma_i)\right)$
  - y_{max}: The maximum fuzzy value for phase part $Max\left(\mu_{gaussian}(HoD_i; m_i, \sigma_i)\right)$
  - $z_{min} = 0$: The minimum interpolation value
  - $z_{max} = 1$: The maximum interpolation value
  Finally, the rule space is present in the following Figure 2:

- **Step 4. Rule generation**
  Aim to reduce the time-consuming of the model; we will group the data with neighbor pixels due to the histogram [37], then determine the rule parameters via the Ternary search [38] and Co-Spatial CFIS+ [27]. The output of this process will produce a new rule base corresponding to the input image.
  Specifically, the process of generating rules directly from the image is described as follows.
  Step 4.1 Define regions (groups of pixels)
  In the case of RSI with a vast number of pixels, processing each pixel will consume a lot of computational time and system resources. Therefore, reducing the data dimension to minimize computation time and system resources is necessary. This study suggests using a histogram [37] to group pixels, then divide pixels into specific regions.
  Step 4.2 Determine the boundary parameters of a rule (a, b, c, a', b', c')
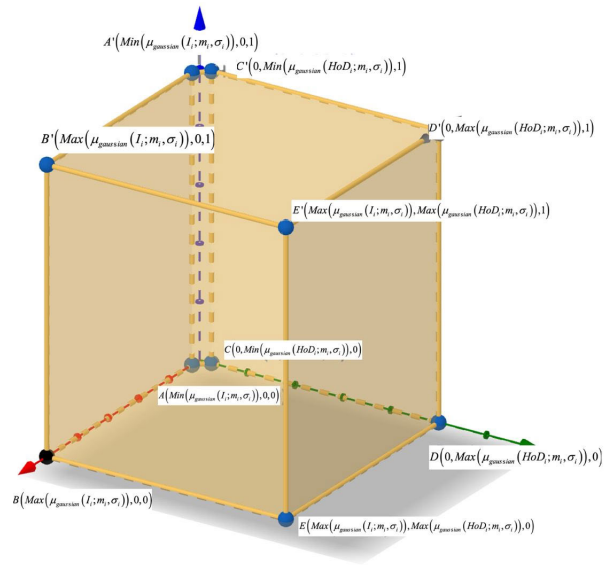

FIGURE 2. Solution space.

Because of using complex fuzzy rulebase of Co-Spatial CFIS+ [27], this step needs to determine the rule parameters such as (a, b, c, a', b', c'):

Step 4.2.1. Determine value (b, b')
The values b and b'' have been established via the Ternary search algorithm [38] as follows:

Step 4.2.2. Determine the value (a, a', c, c')
The values (a, a', c, c') are the boundary parameters and calculate by the following formulas (4-7) [27]:

$$a_j = \frac{\sum\limits_{i=1,2,...,|NP_j| \ and \ X_{ij}^{(k)} \leq b_{ij}} U_{i,j} \times X_{i,j}^{(k)}}{\sum\limits_{i=1,2,...,|NP_j| \ and \ X_{ij}^{(k)} \leq b_{ij}} U_{i,j}} \quad (4)$$

$$a'_j = \frac{\sum\limits_{i=1,2,...,|NP_j| \ and \ HoD_{ij}^{(k)} \leq b_{ij}} U_{i,j} \times HoD_{i,j}^{(k)}}{\sum\limits_{i=1,2,...,|NP_j| \ and \ HoD_{ij}^{(k)} \leq b_{ij}} U_{i,j}} \quad (5)$$

$$c_j = \frac{\sum\limits_{i=1,2,...,|NP_j| \ and \ X_{ij}^{(k)} \geq b_{ij}} U_{i,j} \times X_{i,j}^{(k)}}{\sum\limits_{i=1,2,...,|NP_j| \ and \ X_{ij}^{(k)} \geq b_{ij}} U_{i,j}} \quad (6)$$

$$c'_j = \frac{\sum\limits_{i=1,2,...,|NP_j| \ and \ HoD_{ij}^{(k)} \geq b_{ij}} U_{i,j} \times HOD_{i,j}^{(k)}}{\sum\limits_{i=1,2,...,|NP_j| \ and \ HoD_{ij}^{(k)} \geq b_{ij}} U_{i,j}} \quad (7)$$

where:
- $|NP_j|$: Number of pixel groups of the group j
- $U_{i,j}$: The membership value of the ith pixel in group j
- $X_{i,j}^{(k)}$: The amplitude term of the ith pixel in the group j at time k

---

Algorithm The Ternary Search Algorithm

Input − An sorted array X, range [start, end], and key to find
Output − The position corresponding to the key (If there exists a satisfactory solution)

Begin
1. if start <= end then
2.   midLeft:= (2×start + end)/3
3.   midRight:= (start + 2×end)/3
4.   if X[midLeft] == key then
5.   return midLeft
6.   if X[midRight] == key then
7.   return midRight
8.   If key < X[midLeft] then
9.   call ternarySearch (X, start, midLeft - 1, key)
10.   If key > X[midRight] then
11.   call ternarySearch (X, midSecond + 1, end, key)
12.   else
13.   call ternarySearch (array, midFirst +. 1,   midSecond − 1, key)
14.   else
15.   return invalid location
End

- $HoD_{i,j}^{(k)}$: The phase term of ith pixel in the group j at time k
- **Step 5: Rule review**

Definition 4: Let D be the solution coverage region, V be the domain of the rule space, and D is bounded by:

1) Axis value $ox \in [a, b]$; $a, b \in R^+$
2) The Oy axis is limited by two continuous functions $g_1(x)$ and $g_2(x)$
3) The Oz axis is limited by two continuous functions $f_1(x, y), f_2(x, y)$.

The domain of the rule space V of D is determined by the formula (8) and shown in Figure 3:

$$V = \iiint_D dV$$
$$\Leftrightarrow \int_a^b \int_{g_1(x)}^{g_2(x)} \int_{f_1(x,y)}^{f_2(x,y)} dz\,dy\,dx$$
$$= \int_a^b \int_{g_1(x)}^{g_2(x)} \left(\int_{f_1(x,y)}^{f_2(x,y)} dz \right) dy\,dx. \tag{8}$$

Steps 5.1: Determine the intersection between two rule sapce domains p, q The rule space domain of two rules p, q is specified by the formula (9 - 10) as follows:

$$V_p = \int_{a^p}^{b^p} \int_{g_2^p(x)}^{g_2^p(x)} \left(\int_{f_2^p(x,y)}^{f_2^p(x,y)} dz \right) dy\,dx \tag{9}$$

$$V_q = \int_{a^q}^{b^q} \int_{g_2^q(x)}^{g_2^q(x)} \left(\int_{f_2^q(x,y)}^{f_2^q(x,y)} dz \right) dy\,dx \tag{10}$$

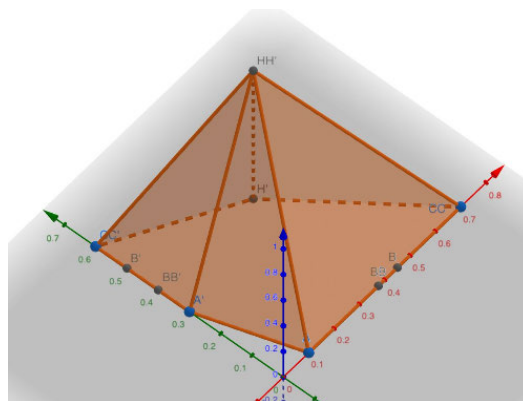We determine the measure of two complex fuzzy rules in the triangular space as the intersection space part

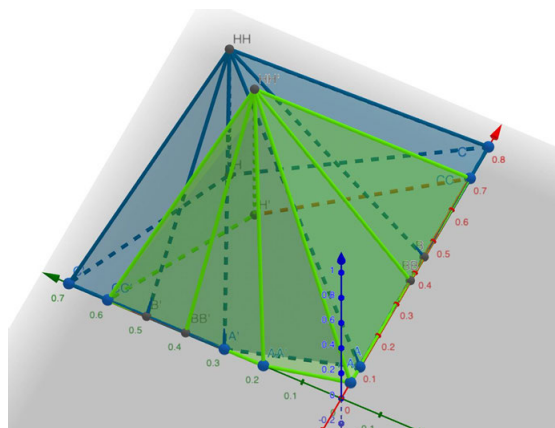**FIGURE 3. Illustrate the rule space domain V.**

FIGURE 4. The intersection space part between the two rules *p*, *q*.

between the two rules p, q due to formula (11) and shown in Figure (4) below:

$$V_{pq} = V_p \cap V_q \tag{11}$$

To determine the value V_{pq} of the intersection domain between two rules, the solution space Ω divided into square blocks according to formula (12) as follows:

$$\Omega_{ijk} = [x_{i-1}, x_i] \times [y_{j-1}, y_j] \times [z_{k-1}, z_k] \tag{12}$$

where
- $x_i \in [x_{\min}, x_{\max}]$, $|x_i - x_{i-1}| = \theta$, $\forall i = 1, 2, \ldots$
- $y_j \in [y_{\min}, y_{\max}]$, $|y_j - y_{j-1}| = \theta$, $\forall i = 1, 2, \ldots$
- $z_i \in [z_{\min}, z_{\max}]$, $|z_i - z_{i-1}| = \theta$, $\forall i = 1, 2, \ldots$
- θ: denote the size of each square block, and it satisfies the conditions in (13).

$$\begin{cases} \left| 1 - \dfrac{V_{actual}}{V_\theta} \right| \le \varepsilon \\ V_{actual} = S_{base\ area} \times h \end{cases} \tag{13}$$

with
- V_{actual}: the actual volume of rule space
- V_θ: is the actual volume of the rule space when calculated by summing the volumes of the squares
- ε: acceptable threshold value of error ($< 5\%$)

- $S_{basearea}$: the bottom area of the rule space R
- h: the height of the rule space R

Steps 5.1.1: Determine the relative position of the square block with the rule space

Since the size of each square block Ω_{ijk} is very small, we consider the center point of each square $G_{ijk}(x_j, y_j, z_k)$ to represent the block. Thus, the problem is finding the center point's relative position G_{ijk} with the rule space V. This step contains the following steps

Steps 5.1.1.1: Consider the first side of the rule space V

Suppose points' coordinates $A(x_A, y_A, z_A)$, $B(x_B, y_B, z_B)$, $C(x_C, y_C, z_C)$ are on the first side of the rule space. The equation of the first side is determined by equation (14)

$$N_a x + N_b y + N_c z + d = 0 \qquad (14)$$

The coefficients (N_a, N_b, N_c) satisfy the following set of equations (15):

$$\begin{cases} N_a \times x_A + N_b \times y_A + N_c \times z_A + d = 0 \\ N_a \times x_B + N_b \times y_B + N_c \times z_B + d = 0 \\ N_a \times x_C + N_b \times y_C + N_c \times z_C + d = 0 \end{cases} \qquad (15)$$

Based on the equation of the first side, the normal vector of the plane has the form: $\vec{N} = (N_a, N_b, N_c)$

Steps 5.1.1.2: Determine whether the point is inside or outside the plane by calculating the dot product of the normal vector with the coordinates of the considered point by the following formula (16):

$$\vec{N} \cdot G_{ijk} = N_a \times x_i + N_b \times y_j + N_c \times z_k \qquad (16)$$

Repeat step 5.1.1.1 and step 5.1.1.2 with all the remaining sides of the solution space domain V and determine the point's relative position G_{ijk} with the rule space V as formula (17). After that, we can specify the square block v in the rule space V.

$$\begin{cases} If \qquad \vec{N} \cdot G_{ijk} < 0, \ G_{ijk} \notin V \\ elsewise, \quad G_{ijk} \in V \end{cases} \qquad (17)$$

Steps 5.1.2: Determine the intersection of two rule spaces

The intersection of two rule spaces (denote V_{pq}) is the set of square blocks Ω_{ijk} in the rule spaces p and q. Therefore, V_{pq} is determined by the following formula:

$$V_{pq} = \sum V_{\Omega_{ikj}} \qquad (18)$$
$$V_{\Omega_{ijk}} = |x_{i-1}, x_i| \times |y_{j-1}, y_j| \times |z_{k-1}, z_k| \qquad (19)$$

where:
- V_{pq}: the volume of the intersection of two rule spaces
- $V_{\Omega_{ijk}}$: the volume of square block Ω_{ijk}

Steps 5.2. Optimizing rule

At this step, we process to optimize the rule, including combining rules, removing rules, or adding rules to obtain a better rule system as follows:

Assuming ε_v is the ratio between the volume of the intersection region and the volume of rule space, ε_R is the ratio factor between the rule's parameters.
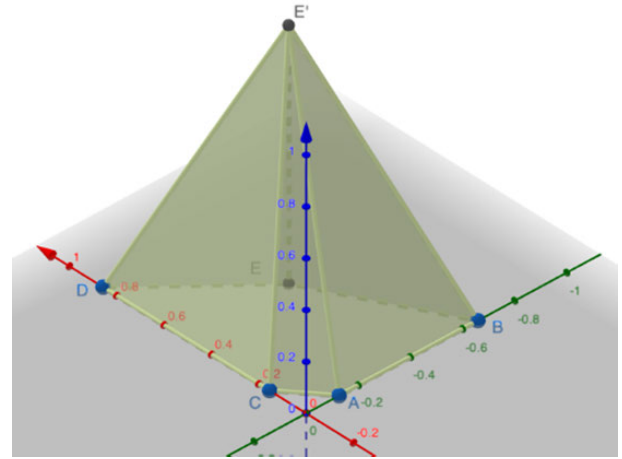

FIGURE 5. New rule space after merging two rules p, q.

- If $\frac{V_{pq}}{V_p} \geq \varepsilon_v$ and $\frac{V_{pq}}{V_q} \geq \varepsilon_v$ and $\frac{a_p}{a_p} + \frac{c_p}{c_p} + \frac{a'_p}{a'_p} + \frac{c'_p}{c'_p} < \varepsilon_R$ then combining the rules:

$$a_{new} = \frac{a_p + a_q}{2}; b_{new} = \frac{b_p + b_q}{2}; b_{new} = \frac{c_p + c_q}{2}$$
$$a'_{new} = \frac{a'_p + a'_q}{2}; b'_{new} = \frac{b'_p + b'_q}{2}; b'_{new} = \frac{c'_p + c'_q}{2}$$

The new rule space after merging two rules as (5) follows:
- If $\frac{V_{pq}}{V_q} \geq \varepsilon_v$ and $\frac{V_{pq}}{V_p} < \varepsilon_v$ and $\frac{a_p}{a_p} + \frac{c_p}{c_p} < \varepsilon_R$ or $\frac{a'_p}{a'_p} + \frac{c'_p}{c'_p} < \varepsilon_R$ Then remove the rule q.
- If $\frac{V_{pq}}{V_q} < \varepsilon_v$ and $\frac{V_{pq}}{V_p} \geq \varepsilon_v$ and $\frac{a_p}{a_p} + \frac{c_p}{c_p} < \varepsilon_R$ or $\frac{a'_p}{a'_p} + \frac{c'_p}{c'_p} < \varepsilon_R$ Then remove the rule p.
- If $\frac{V_{pq}}{V_q} < \varepsilon_v$ and $\frac{V_{pq}}{V_p} < \varepsilon_v$ Then use both rules p and q.

After evaluating all pairs of rules, we obtain the rule base generated from the new image R'.

- **Step 6: Synthesize the old rulebase R and new rulebase R'**

  In this step, we will compare each rule of the new rulebase with the rules of the old rulebase using the intersection of the rulebase in step 5.

C. AN EXAMPLE OF THE PROPOSED METHOD

Let us take a working example to comprehend the intuition behind this model.

- **Step 1. Preprocessing input data**

  Input data includes:
  - I_0: The last image (the most recent image) in the training set
  - I_1: The first image in the new album

- **Step 1.1: Convert image from color image to gray image**

  Use the method of converting from a color remote sensing image to gray according to the formula (20) below:

$$Y = 0.2126R + 0.7152G + 0.0722B \qquad (20)$$

TABLE 1. The most recent image in the training set (I_0).

4	95	235	205	128	166	74	15	59
109	209	234	84	114	151	214	168	247
145	64	113	90	175	29	68	202	124
79	202	130	220	133	148	190	159	222
88	52	57	221	224	100	92	164	55
170	230	118	215	242	16	175	215	128
231	123	123	143	25	153	4	96	1
68	90	103	172	69	195	144	38	70
0	29	88	46	244	218	134	242	24

TABLE 2. The first image in the new training set (I_1).

195	179	4	235	231	168	21	169	245
198	97	116	39	238	41	102	105	183
59	96	208	35	170	254	157	125	56
184	8	104	51	11	231	188	60	226
234	121	179	240	77	77	128	65	226
237	209	224	76	186	54	73	215	210
141	170	161	204	202	77	197	145	233
49	26	222	48	13	169	196	248	157
143	174	18	40	88	186	153	183	109

TABLE 3. The imaginary part HoD_1.

191	84	231	30	103	2	53	154	186
89	112	118	45	124	110	112	63	64
86	32	95	55	5	225	89	77	68
105	194	26	169	122	83	2	99	4
146	69	122	19	147	23	36	99	171
67	21	106	139	56	38	102	0	82
90	47	38	61	177	76	193	49	232
19	64	119	124	56	26	52	210	87
143	145	70	6	156	32	19	59	85

TABLE 4. Image I_0 representation in range [0,1].

0.016	0.373	0.922	0.804	0.502	0.651	0.29	0.059	0.231
0.427	0.82	0.918	0.329	0.447	0.592	0.839	0.659	0.969
0.569	0.251	0.443	0.353	0.686	0.114	0.267	0.792	0.486
0.31	0.792	0.51	0.863	0.522	0.58	0.745	0.624	0.871
0.345	0.204	0.224	0.867	0.878	0.392	0.361	0.643	0.216
0.667	0.902	0.463	0.843	0.949	0.063	0.686	0.843	0.502
0.906	0.482	0.482	0.561	0.098	0.6	0.016	0.376	0.004
0.267	0.353	0.404	0.675	0.271	0.765	0.565	0.149	0.275
0	0.114	0.345	0.18	0.957	0.855	0.525	0.949	0.094

TABLE 5. Image I_1 representation in range [0,1].

0.765	0.702	0.016	0.922	0.906	0.659	0.082	0.663	0.961
0.776	0.38	0.455	0.153	0.933	0.161	0.4	0.412	0.718
0.231	0.376	0.816	0.137	0.667	0.996	0.616	0.49	0.22
0.722	0.031	0.408	0.2	0.043	0.906	0.737	0.235	0.886
0.918	0.475	0.702	0.941	0.302	0.302	0.502	0.255	0.886
0.929	0.82	0.878	0.298	0.729	0.212	0.286	0.843	0.824
0.553	0.667	0.631	0.8	0.792	0.302	0.773	0.569	0.914
0.192	0.102	0.871	0.188	0.051	0.663	0.769	0.973	0.616
0.561	0.682	0.071	0.157	0.345	0.729	0.6	0.718	0.427

TABLE 6. Image HoD_1 representation in range [0,1].

0.749	0.329	0.906	0.118	0.404	0.008	0.208	0.604	0.73
0.349	0.44	0.463	0.176	0.486	0.431	0.439	0.247	0.251
0.338	0.125	0.373	0.216	0.019	0.882	0.349	0.302	0.266
0.412	0.761	0.102	0.663	0.479	0.326	0.008	0.389	0.015
0.573	0.271	0.478	0.074	0.576	0.09	0.141	0.388	0.67
0.262	0.082	0.415	0.545	0.22	0.149	0.4	0	0.322
0.353	0.185	0.149	0.239	0.694	0.298	0.757	0.193	0.91
0.075	0.251	0.467	0.487	0.22	0.102	0.204	0.824	0.341
0.561	0.568	0.274	0.023	0.612	0.126	0.075	0.231	0.333

TABLE 7. The result of the fuzzied amplitude term of the image I_1.

0.763	0.874	0.185	0.444	0.475	0.933	0.273	0.929	0.371
0.742	0.841	0.947	0.392	0.422	0.407	0.874	0.892	0.848
0.546	0.835	0.661	0.363	0.924	0.311	0.975	0.978	0.524
0.841	0.203	0.886	0.483	0.218	0.475	0.815	0.555	0.515
0.451	0.966	0.874	0.407	0.693	0.693	0.986	0.596	0.515
0.43	0.652	0.532	0.685	0.829	0.507	0.661	0.604	0.644
1	0.924	0.963	0.693	0.71	0.693	0.748	0.998	0.459
0.467	0.304	0.546	0.459	0.229	0.929	0.755	0.349	0.975
0.999	0.904	0.257	0.4	0.778	0.829	0.986	0.848	0.913

TABLE 8. The result of the fuzzied imaginary term of the image HoD_1.

0.233	0.995	0.058	0.599	0.976	0.331	0.823	0.557	0.267
1	0.932	0.894	0.747	0.848	0.945	0.934	0.901	0.908
0.998	0.617	0.996	0.84	0.355	0.074	1	0.976	0.932
0.968	0.213	0.557	0.41	0.863	0.993	0.331	0.988	0.346
0.638	0.939	0.865	0.485	0.63	0.526	0.659	0.989	0.393
0.926	0.505	0.965	0.71	0.848	0.679	0.98	0.314	0.991
1	0.769	0.679	0.886	0.34	0.972	0.22	0.788	0.056
0.488	0.908	0.886	0.846	0.848	0.557	0.814	0.127	0.999
0.669	0.651	0.944	0.364	0.536	0.62	0.488	0.871	0.996

where:
- Y: gray matrix to find
- R: the red-gray matrix of the image
- G: the green-gray matrix of the image
- B: the blue-gray matrix of the image

- **Step1.2: Determine the phase part (HoD)**
  After applying formula (1) the phase part of the images I_1 and I_0 has the following results.
- **Step 1.3: Transform the amplitude and phase part of the image to [0,1]**
  Gray image has the largest value of 255, so to convert to [0,1], by dividing each pixel value by 255, we get the (4, 5, 6) the following result:
  From there, the input data to process the following steps has the following form: $X_1 (I_1, HoD_1)$
- **Step 2: Fuzzification Process**

The amplitude term I_1.
- The fuzzy value corresponding to the amplitude and phase term of image I_1 is calculated using the Gaussian membership function (2) as follows:

$$\mu_{gaussian}(I_1; m_I, \sigma_I) = e^{-\frac{1}{2}\left(\frac{I_1 - m_I}{\sigma_I}\right)^2}$$

With the amplitude term of image I_1, the standard deviation of pixel intensities $\sigma_I = 0.291$ and $m_I = 0.551$ the obtained fuzzied value is shown in Table 7

The calculation is the same as for the amplitude part of the image, the Gaussian function (2) is used to calculate the phase part (HoD_1) with the standard deviation $\sigma_{HoD} = 0.232$ and $m_{HoD} = 0.353$. The results are represented in Table 8
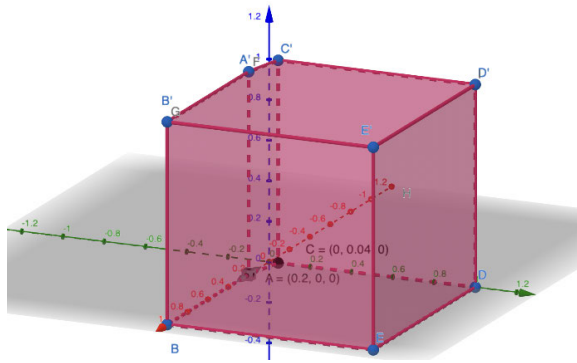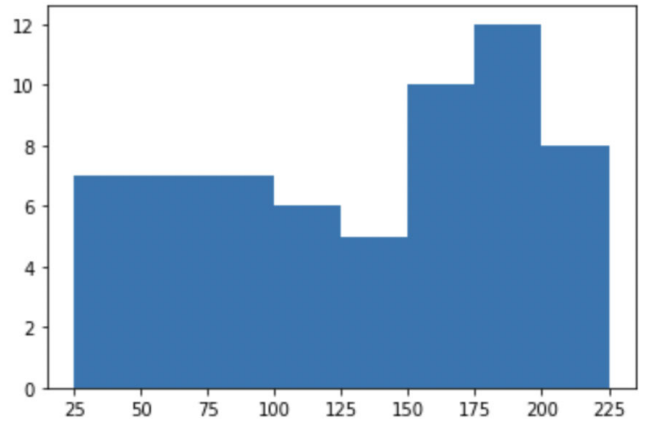
FIGURE 6. The solution space of image I_1.

FIGURE 7. Histogram of the input image.

- **Step 3: Determine the solution space**

  After the fuzzification process, solution space Ω is determined by applying formula (3) specifically as follows:

  $$Min \left(\mu_{gauss\,ian} \left(I_i; m_i, \sigma_i \right) \right) = 0.185;$$
  $$Max \left(\mu_{gauss\,ian} \left(I_i; m_i, \sigma_i \right) \right) = 1$$
  $$Min \left(\mu_{gauss\,ian} \left(HoD_i; m_i, \sigma_i \right) \right) = 0.056;$$
  $$Max \left(\mu_{gauss\,ian} \left(HoD_i; m_i, \sigma_i \right) \right) = 1$$

  Then, the coordinates of the points A, B, C, D, E A', B', C', E respectively are determined as follows:

  $$A : \left(Min \left(\mu_{gauss\,ian} \left(I_i; m_i, \sigma_i \right) \right), 0, 0 \right)$$
  $$B : \left(Max \left(\mu_{gauss\,ian} \left(I_i; m_i, \sigma_i \right) \right), 0, 0 \right)$$
  $$C : \left(0, Min \left(\mu_{gauss\,ian} \left(HoD_i; m_i, \sigma_i \right) \right), 0 \right)$$
  $$D : \left(0, Max \left(\mu_{gauss\,ian} \left(HoD_i; m_i, \sigma_i \right) \right), 0 \right)$$
  $$E : \left(Max \left(\mu_{gauss\,ian} \left(I_i; m_i, \sigma_i \right) \right), \right.$$
  $$\left. Max \left(\mu_{gauss\,ian} \left(HoD_i; m_i, \sigma_i \right) \right), 0 \right)$$
  $$A' : \left(Min \left(\mu_{gauss\,ian} \left(I_i; m_i, \sigma_i \right) \right), 0, 1 \right)$$
  $$B' : \left(Max \left(\mu_{gauss\,ian} \left(I_i; m_i, \sigma_i \right) \right), 0, 1 \right)$$
  $$C' : \left(0, Min \left(\mu_{gauss\,ian} \left(HoD_i; m_i, \sigma_i \right) \right), 1 \right)$$
  $$D' : \left(0, Max \left(\mu_{gauss\,ian} \left(HoD_i; m_i, \sigma_i \right) \right), 1 \right)$$
  $$E' : \left(Max \left(\mu_{gauss\,ian} \left(I_i; m_i, \sigma_i \right) \right), \right.$$
  $$\left. Max \left(\mu_{gauss\,ian} \left(HoD_i; m_i, \sigma_i \right) \right), 1 \right)$$

  The solution space is bounded by the set of points A, B, C, D, E, A', B', C', E as shown in Figure 6.

- **Step 4: Establish the rule base**

  Step 4.1. Determine the regions (the group of pixels in the image)

  With input image I_1, assuming we choose the number of regions to 10, we have the histogram in 10 data areas, as shown in Figure 7.

  From the histogram results, label the pixels corresponding to the groups described in Table 8.

  Steps 4.2. Determine the boundary point of a rule (a, b, c, a', b', c')

  With the results obtained in **step 4.1**, the corresponding values in each region are as follows::

FIGURE 8. Results of labeling groups according to Histogram.

- Region 1: {(0.185,0.058), (0.273, 0.823), (0.203, 0.213), (0.311, 0.074), (0.218, 0.863), (0.229, 0.848), (0.257, 0.944)}
- Region 2: {(0.392, 0.747), (0.407, 0.945), (0.363, 0.84), (0.467, 0.488), (0.304, 0.908), (0.459, 0.846), (0.4, 0.364)}
- Region 3: {(0.546, 0.998), (0.524, 0.932), (0.483, 0.41), (0.555, 0.988), (0.596, 0.989), (0.507, 0.679), (0.661, 0.98)}
- Region 4: {(0.841, 0.932), (0.835, 0.617), (0.693, 0.63), (0.693, 0.526), (0.685, 0.71), (0.693, 0.972), (0.778, 0.536)}
- Region 5: {(0.947, 0.895), (0.874, 0.934), (0.892, 0.901), (0.978, 0.976), (0.886, 0.957), (0.966, 0.939), (0.913, 0.996)}
- Region 6: {(0.986, 0.659), (1, 1), (0.998, 0.788), (0.999, 0.669)}
- Region 7: {(0.933, 0.331), (0.929, 0.557), (0.924, 0.355), (0.975, 1), (0.924, 0.769), (0.963, 0.679), (0.929, 0.557), (0.904, 0.651), (0.986, 0.488)}
- Region 8: {(0.763, 0.233), (0.874, 0.995), (0.742, 1), (0.848, 0.908), (0.841, 0.968), (0.815, 0.331), (0.874, 0.865), (0.829, 0.848), (0.748, 0.22), (0.755, 0.814), (0.829, 0.62), (0.848, 0.871)}

- Region 9: {(0.661, 0.996), (0.652, 0.505), (0.532, 0.965), (0.604, 0.314), (0.644, 0.991), (0.693, 0.886), (0.71, 0.34), (0.546, 0.886)}
- Region 10: {(0.444, 0.599), (0.475, 0.976), (0.371, 0.267), (0.422, 0.848), (0.475, 0.993), (0.515, 0.346), (0.451, 0.638), (0.407, 0.485), (0.515, 0.393), (0.43, 0.926), (0.459, 0.056), (0.349, 0.127)}}

Steps 4.2.1. Determine the rule parameters (b, b')

Applying the Ternary search algorithm [29]:
- Region 1: $(b, b') = (0.185, 0.185)$
- Region 2: $(b, b') = (0.392, 0.407)$
- Region 3: $(b, b') = (0.546, 0.524)$
- Region 4: $(b, b') = (0.685, 075)$
- Region 5: $(b, b') = (0.978, 1)$
- Region 6: $(b, b') = (1, 1)$
- Region 7: $(b, b') = (0.986, 01901)$
- Region 8: $(b, b') = (0.763, 0.874)$
- Region 9: $(b, b') = (0.532, 0.62)$
- Region 10: $(b, b') = (0.444, 0.475)$

Steps 4.2.2. Determine the rule parameters a, a' and c, c'

The rule parameter a, a' and c, c' are obtained using the formula (4-7) as follows:

$$a_1 = \frac{\sum\limits_{i=1,2, ...,|NP_1| \ and \ X_{i1}^{(k)} \leq b_{i1}} U_{i,1} \times X_{i,1}^{(k)}}{\sum\limits_{i=1,2, ...,|NP_1| \ and \ X_{i1}^{(k)} \leq b_{i1}} U_{i,1}} = 0.423$$

$$a'_1 = \frac{\sum\limits_{i=1,2, ...,|NP_1| \ and \ HoD_{i1}^{(k)} \leq b_{ij}} U_{i,1} \times HOD_{i,1}^{(k)}}{\sum\limits_{i=1,2, ...,|NP_1| \ and \ HoD_{i1}^{(k)} \leq b_{i1}} U_{i,1}}$$
$$= 0.354$$

$$c_1 = \frac{\sum\limits_{i=1,2, ...,|NP_1| \ and \ X_{i1}^{(k)} \geq b_{i1}} U_{i,1} \times X_{i,1}^{(k)}}{\sum\limits_{i=1,2, ...,|NP_1| \ and \ X_{i1}^{(k)} \geq b_{i1}} U_{i,1}} = 0.784$$

$$c'_1 = \frac{\sum\limits_{i=1,2, ...,|NP_1| \ and \ HoD_{i1}^{(k)} \geq b_{i1}} U_{i,1} \times HOD_{i,1}^{(k)}}{\sum\limits_{i=1,2, ...,|NP_1| \ and \ HoD_{i1}^{(k)} \geq b_{i1}} U_{i,1}}$$
$$= 0.778$$

Thus, the rule corresponding to region 1 is created by the parameters $(a_1, a'_1, c_1, c'_1) = (0.423, 0.712, 0.784, 0.354, 0.739, 0.788)$ as shown in Figure 9

Repeat the same with region 2; we get $(a_2, a'_2, c_2, c'_2) = (0.132, 0.423, 0.817, 0.265, 0.673, 0.882)$ and describe in Figure 10.

We continue the above steps until all areas or groups of pixels are exhausted.

- **Step 5: Rule review**

  Step 5.1: Determine the intersection of the solution region created by two rules p, q
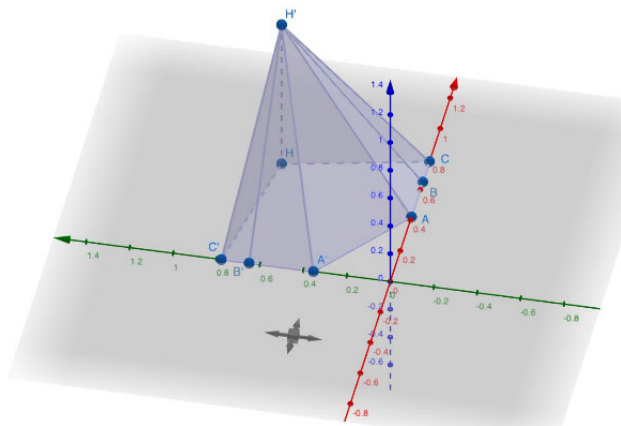

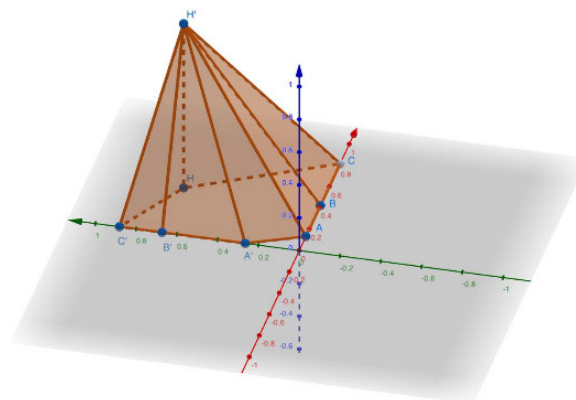**FIGURE 9.** Solution space 1 corresponds to region 1.

FIGURE 10. Solution space 1 corresponds to region 2.

From the two rules obtained corresponding to regions 1 and 2 in the previous step, the volume of the intersection space of the two rule regions is based on **steps 5.1.1, 5.1.2**. We get the following results:

Region 1:
- Actual volume: $V_{actual(1)=0.0242}$;
- Square block size: $\theta = 0.01$;
- The volume of the square block: $V_{\theta(1)} = 0.0239$;
- Threshold value: $\varepsilon = 0.05$

$$\left| 1 - \frac{V_{actual(1)}}{V_{\theta(1)}} \right| = \left| 1 - \frac{0.0242}{0.0239} \right| = 0.013 < \varepsilon$$

Region 2:
- Actual volume: $V_{actual(2)=0.0116}$;
- Square block size: $\theta = 0.01$;
- The volume of the square block: $V_{\theta(2)} = 0.0112$;
- Threshold value: $\varepsilon = 0.05$

$$\left| 1 - \frac{V_{actual(2)}}{V_{\theta(2)}} \right| = \left| 1 - \frac{0.0116}{0.0112} \right| = 0.036 < \varepsilon$$

Finally, the intersection of the solution region is specified: $V_{(1)(2)} = V_{\theta(1)} \cap V_{\theta(2)} = 0.00176$

Steps 5.2. Optimizing rule

For the given input image example, suppose $\varepsilon_v = 0.8$, $\varepsilon_R = 0.5$, We have:

$$\frac{V_{(1)(2)}}{V_{(1)}} = \frac{0.00176}{0.0242} = 0.074 < \varepsilon_v$$

$$\frac{V_{(1)(2)}}{V_{(2)}} = \frac{0.00176}{0.0116} = 0.157 < \varepsilon_v$$

Hence using both rules 1 and 2.

- **Step 6: Synthesize the old and new system of rules**
  From step 5, we get the rule system after being evaluated and reduced. Then, the proceeds combine these rules with those obtained from the Co-Spatial CFIS+ system to infer the following image result.

V. REAL EXAMPLE RESULTS

To demonstrate the effectiveness and merit in improving the efficiency of the rule base of Co-Spatial CFIS+, this section shows experiments for implementation comparisons in change prediction in RSI. The proposed Adaptive Spatial CFIS method is compared with other state-of-art methods, including SeriesNet [40], Deep Slow Feature Analysis (DSFA) [41], PFC-PFR [42], and Co-Spatial CFIS+ [27]. The evaluation criteria are used to estimate RMSE, R2, computational time, and the number of rules.

A. EXPERIMENTAL DATA

Collection of time series satellite images collected from the US Navy's weather image database [39] at specific locations and periods. The dataset used in the study consisted of more than 12,000 images of 500×500 size with a 30-minute interval between two consecutive images at three different locations, the Gulf of Mexico (Data 3), the Pacific Coast (Data 2), the US pacific, and regions of Hawaii (Data 1).

Our proposed model split the dataset to adopt a 7:3 ratio, allocating 70% of the data for training and the remaining 30% for testing. After determining the appropriate parameters of the proposed methods, the model presents the results of the first five prediction images to show the effectiveness of the proposed method in predicting time series satellite images.

B. EXPERIMENTAL TOOLS

We have experimented the proposed method and related methods on a virtualized server system with three physical server nodes; each physical server node has CPU: 2.0 GHz, RAM: 384 Gb, and Hard Drive: 1 T.B.

C. RESULTS AND DISCUSSION

Figure 11 describes in detail the RMSE value corresponding to the prediction process for each image. At the same time, Figure 12 visually compares the average RMSE value for each image on three datasets. As shown in the above figures, it can observe that the Adaptive spatial CFIS++ has a significant improvement over the baseline for predicting five images. The RMSE evaluation index clearly shows the Adaptive spatial CFIS++ has a substantial improvement in accuracy, and the cumulative error decreases gradually along the forecasted image series. Actually, on the first three images, the prediction results of the proposed method and the Co-Spatial CFIS+ are almost no different and are equivalent. The RMSE index obtained when predicting the first image on dataset 1 is nearly 3% lower than that of Co-Spatial CFIS+ at most, while the RMSE result of the proposed method in image 3 seems to be higher than about 1%. With data set 2, the proposed method's first 2 image prediction results give the best results, but the third image is slightly worse than Co-Spatial CFIS+.

Compared with the remaining three methods, the RMSE values of the proposed method are much better on data 1 and data 2. Primarily, the results are obtained with the first image of the image dataset 1 reduced to about 42%, 43%, and 47% compared with the values obtained by three methods Seriesnet, DSFA, and PFC-PFR. Even though the forecast results of the second image on data 1 and 2 of the 3 methods have improved and slightly increased, but still worse than the forecast results applying the proposed method. For the second and third images on the 3rd dataset, the DSFA is the most effective model, with the obtained RMSE index of 6,705 and 7,129, respectively. This result is 7 to 8% higher than the proposed method. However, as mentioned above, the advantage of the proposed model is evident in the reduction of forecast errors accumulated over time for the forecasting process. For that reason, the prediction results of the proposed approach give the best results for the fourth and fifth images on all three data sets. The RMSE values obtained when predicting the fourth and fifth images on 3 data sets are (6,954; 6,396; 7,860) and (7,676; 6,770; 8,231), respectively. This result is much reduced compared with the Co-Spatial+ method or the method using DSFA deep learning.

Apart from using RMSE to evaluate the performance of the five methods, the values of R2 are presented in Figures 13 and 14. The R^2 index is assessed to check the strength of the relationship between the proposed model and the datasets. Figures 13 and 14 describe the R^2 index corresponding to predicting five images in detail. As shown in Figure 13, the obtained R^2 of Adaptive CFIS++ would always be more remarkable, such as above 0.9. These values suggest no dissimilarities between the five images and show a high correlation. For the purpose of demonstrating the stability of the regression model, experimental results on three data sets evaluated on the R^2 index are introduced to demonstrate the strength of the proposed model. Although the number of parameters of the model is very large, the stability of the model is still guaranteed because the R^2 value has very high reliability and is quite similar compared to the remaining models.

Figure 16 shows the comparative results in terms of computational time of the proposed method and SeriesNet, DSFA, PFC-PFR, and Co-Spatial CFIS+ methods on all 3 datasets. As shown in Figure 16, we have the total processing time of the proposed method less than the Co-Spatial CFIS+ method (34%), SeriesNet (37%), DSFA (37%), and significantly less than the PFC-PFR method (55%). The following

Data	SeriesNet					DSFA					PFC-PFR					Co-SPATIAL CFIS+					Proposed method				
	FI (1)	FI (2)	FI (3)	FI (4)	FI (5)	FI (1)	FI (2)	FI (3)	FI (4)	FI (5)	FI (1)	FI (2)	FI (3)	FI (4)	FI (5)	FI (1)	FI (2)	FI (3)	FI (4)	FI (5)	FI (1)	FI (2)	FI (3)	FI (4)	FI (5)
Data 1	7.359	7.187	7.221	8.977	10.045	7.190	7.183	7.485	9.521	10.985	6.709	8.306	11.050	14.562	18.791	3.045	6.219	6.846	7.891	9.239	3.126	6.339	6.796	6.954	7.676
Data 2	6.877	7.032	7.168	8.470	10.007	5.668	6.357	6.763	8.274	9.655	6.932	8.395	11.323	15.210	18.690	5.497	5.785	6.104	6.759	7.645	5.483	5.738	6.240	6.396	6.770
Data 3	7.143	7.406	7.697	8.917	10.882	6.639	6.705	7.129	8.625	10.664	6.933	8.357	11.477	14.626	18.202	6.430	7.059	7.620	8.698	9.695	6.458	7.196	7.701	7.860	8.231

Note:
- FI: Forecast image (1-5)

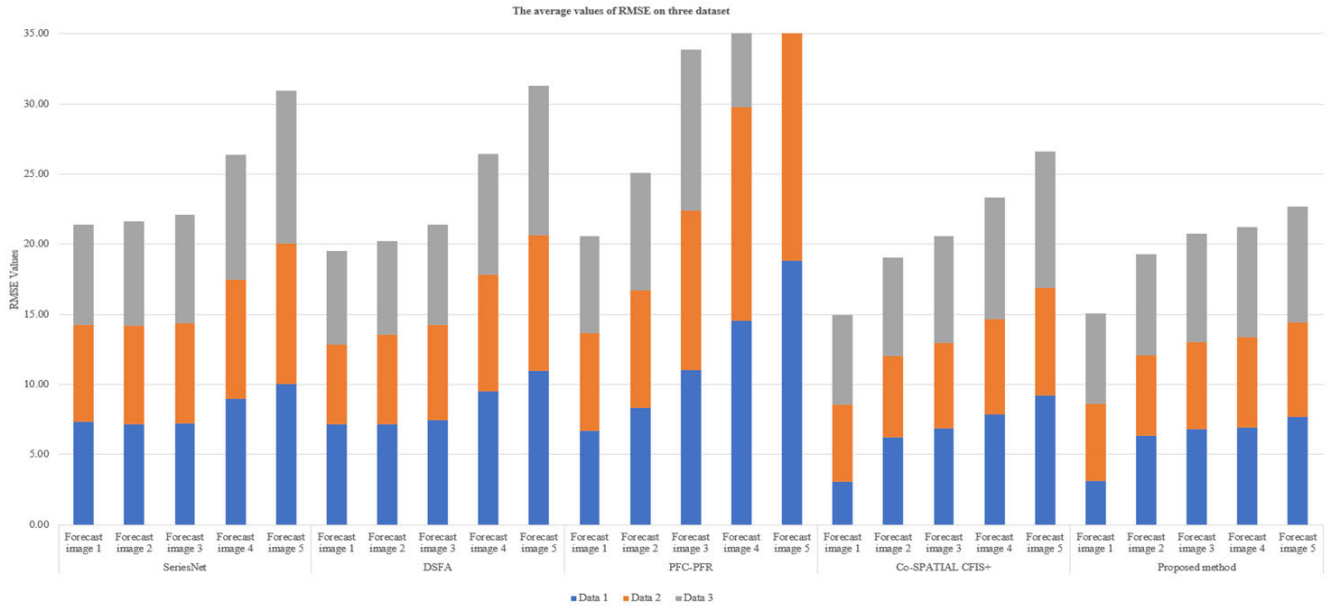**FIGURE 11.** The average values of RMSE on three datasets.

FIGURE 12. The average values of RMSE on three datasets.

Data	SeriesNet					DSFA					PFC-PFR					CO-SPATIAL CFIS +					Proposed method				
	FI (1)	FI (2)	FI (3)	FI (4)	FI (5)	FI (1)	FI (2)	FI (3)	FI (4)	FI (5)	FI (1)	FI (2)	FI (3)	FI (4)	FI (5)	FI (1)	FI (2)	FI (3)	FI (4)	FI (5)	FI (1)	FI (2)	FI (3)	FI (4)	FI (5)
Data 1	0.948	0.934	0.923	0.922	0.915	0.932	0.924	0.919	0.918	0.913	0.934	0.915	0.892	0.890	0.897	0.980	0.975	0.966	0.963	0.960	0.964	0.961	0.966	0.967	0.966
Data 2	0.969	0.969	0.931	0.933	0.931	0.950	0.941	0.942	0.937	0.935	0.958	0.940	0.926	0.935	0.948	0.987	0.983	0.980	0.982	0.981	0.966	0.961	0.961	0.959	0.963
Data 3	0.983	0.983	0.979	0.978	0.965	0.963	0.960	0.957	0.940	0.936	0.972	0.964	0.958	0.959	0.963	0.984	0.983	0.981	0.978	0.976	0.960	0.959	0.964	0.967	0.966

Note:
- FI: Forecast image (1-5)

FIGURE 13. Table the average values of R^2 on each dataset among five compared methods.

two reasons easily explain this result: the proposed method allows generating rules directly from new images without using traditional FCM; Furthermore, the improved method is suggested with the new rulebase to establish an adaptive rulebase through comparisons between two rulebases. Comparing the two rulebases has significantly reduced the number of necessary rules generated in the forecasting process. And especially the new rule system has a better fit with the latest forecast image, leading to a reduction in the cumulative error when forecasting time series images.

From the results mentioned above, the proposed method has obtained almost equivalent accuracy results on different data sets and forecast images compared to related works,

TABLE 9. Results of computational time comparison on three datasets.

Data	SeriesNet	DSFA	PFC-PFR	Co-SPATIAL CFIS+	Proposed method
Data 1	1.582	1.487	1.900	1.510	0.986
Data 2	1.501	1.519	2.223	1.364	0.967
Data 3	1.423	1.508	2.243	1.423	0.887

including Co-Spatial CFIS+, DSFA, SeriesNet, and PFC-PFR. It is better than Co-Spatial CFIS+ slightly compared to other methods.

For R^2 results, the proposed method has worse consequences than Co-spatial or SeriesNet at some forecasting
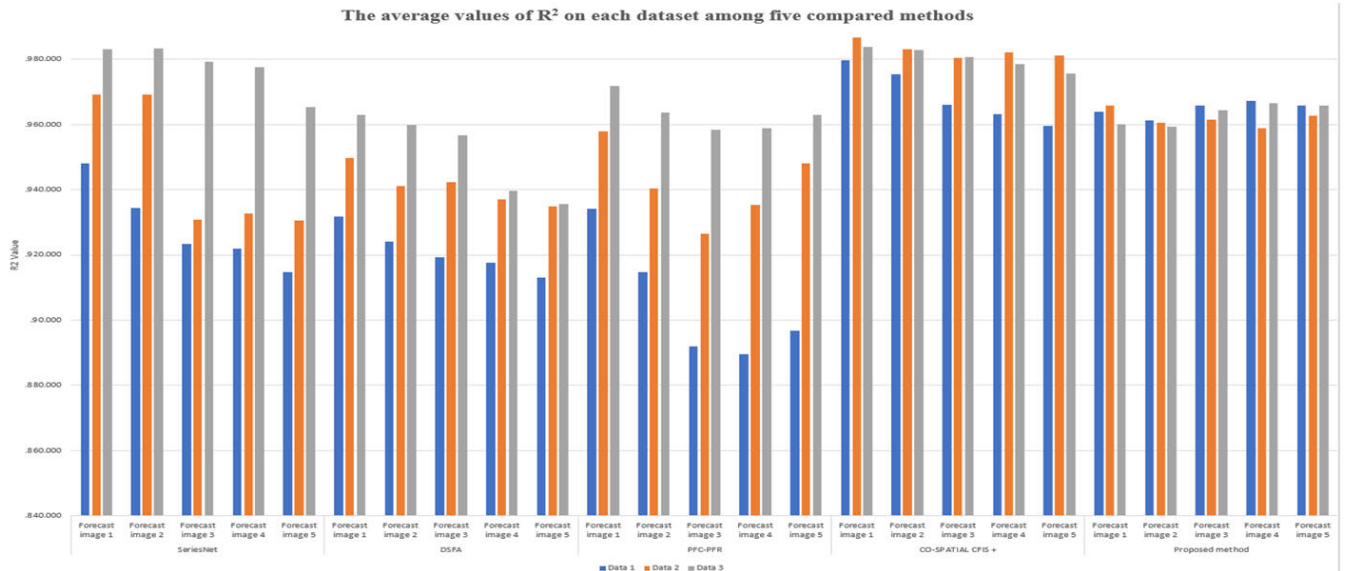
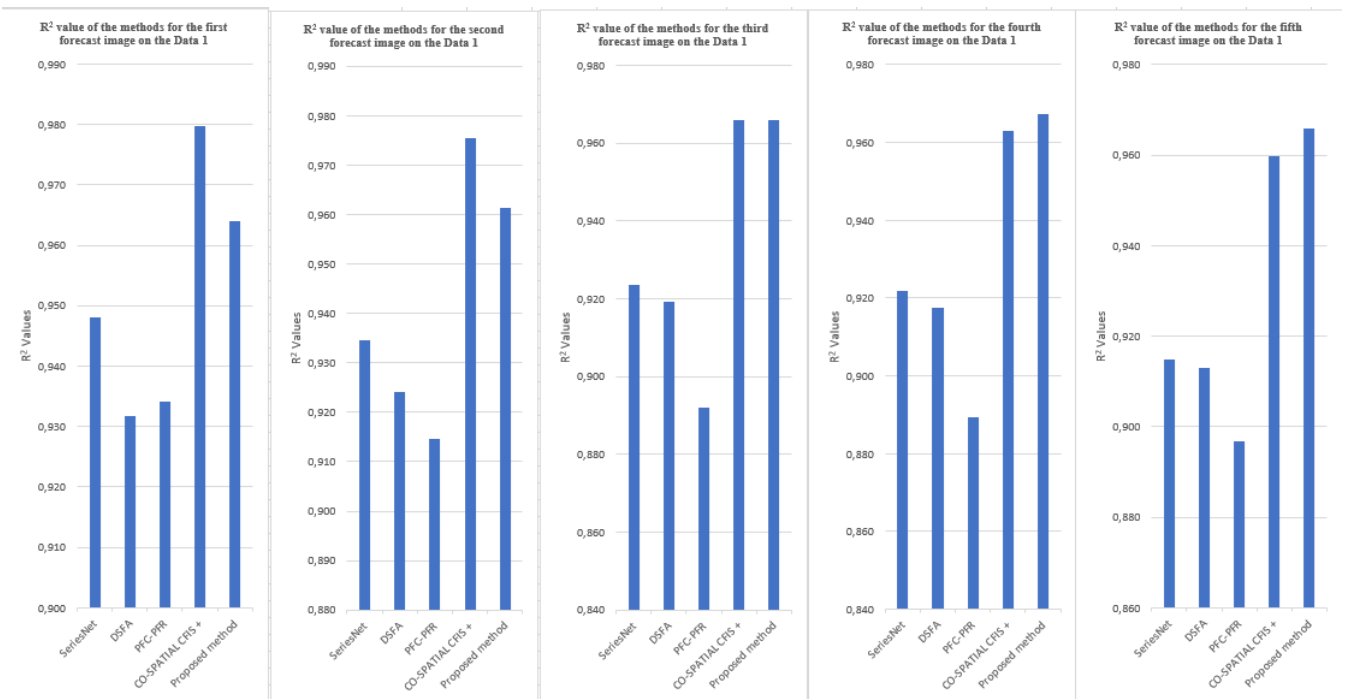**FIGURE 14.** The average values of R^2 on each dataset among five compared methods.

FIGURE 15. R^2 values of the methods for the Data 1.

time. Still, the proposed method's results have stability between forecast images and data sets. The separation of the rule generation process after forecasting a new photo significantly affects this predicting process. Instead of being updated via Co-spatial CFIS+, the rulebase is updated directly through each new image. This latest prediction has dramatically reduced the reliability of the model. But the The model's final result is stable between the forecast images and the data sets. This will help the model, when

TABLE 10. Number of rules of PFC-PFR, Co-Spatial CFIS+, and Proposed methods on three datasets.

Data	PFC-PFR	Co-SPATIAL CFIS+	Proposed method
Data 1	120	48	66
Data 2	115	48	64
Data 3	124	48	68

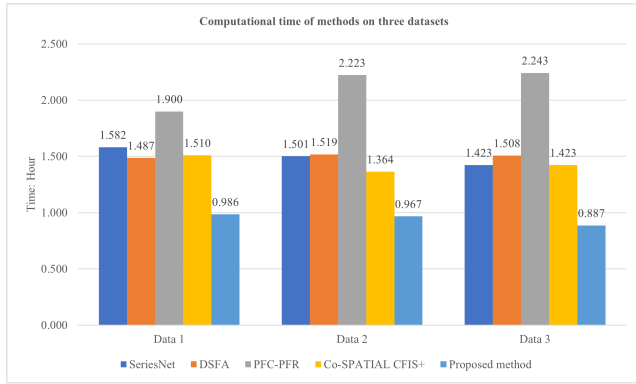extended to other datasets will, still retain the necessary reliability.

FIGURE 16. Computational time of methods on three datasets.

TABLE 11. Detail rules of Proposed methods on three datasets.

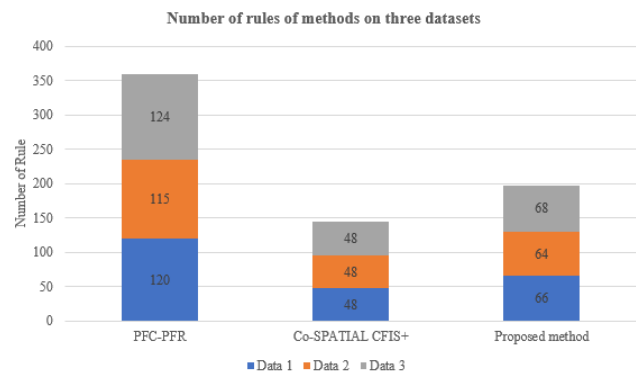| Data	The previous rule generated by Co-Spatial CFIS+	The rules generate directly from the newly obtained images before pruning	The rules generate directly from the newly obtained images after pruning	Total of Rules
Data 1	48	30	18	66
Data 2	48	30	16	64
Data 3	48	30	20	68

FIGURE 17. Number of rules of methods on three datasets.

Figure 17 shows the comparison results with 2 PFC-PFR and Co-SpatialFIS methods on the number of rules on 3 datasets. It is clear that the number of rules of the proposed model is less than on the PFC-PFR on 3 datasets. The number of rules compared to PFC-PFR for each dataset is reduced by 54, 51, and 56, respectively. However, the number of rules has increased compared with Co-spatial by more than 30%. But the goal of the proposed model is to decrease the accumulation of errors and the computation time. However, the accuracy of the prediction model is still maintained within the acceptable threshold.

The proposed method shows superior efficiency compared to related methods in terms of computational time. Previously, for Co-spatial CFIS+, the factor that most affected the time-consuming of the model was the FCM clustering

TABLE 12. ANOVA analysis for values of RMSE.

Source of Variation	SS	df	MS	F	P-Value	F crit
Datasets	1.48	2	0.74	3.22	0.09434	4.46
Models	54.92	4	13.73	59.51	0.00001	3.84
Error	2.40	8	0.30			
Total	11.38	14				

TABLE 13. ANOVA analysis for values of R^2.

Source of Variation	SS	df	MS	F	P-Value	F crit
Datasets	0.002	2	0.0011	6.439	0.0216	4.459
Models	0.004	4	0.0009	5.343	0.0215	3.838
Error	0.001	8	0.0002			
Total	0.007	14				

process. In addition, after predicting a new image, this clustering process has to execute repeat from the beginning, even though only 1 new photo is added to the dataset. By changing the way of producing rules when dealing with a new image, a method to establish rules directly from images is proposed. In addition, the measure between two rule spaces is suggested to evaluate and optimize the rulebase. These ideas led to reducing the model's processing process. Although the processing time is significantly reduced, it does not change the model's accuracy. This result shows the initial effectiveness of directly proposing a rule generation mechanism from the image and using the complex fuzzy measure in space to estimate and determine an adaptive rulebase to include in predicting the following photos.

D. ANOVA ANALYSIS

Based on the experimental results, the two-way ANOVA with $\alpha = 0.05$ was applied to the values of RMSE, R^2, and running time. In this analysis, two null hypotheses in this analysis are:

H_0 : There is no difference between the means of three data sets

H_1: There is no difference between the means of the five models

RMSE: Using two-way ANOVA without replication, the results are presented as in Table 12.

From the results in Table 12, the P-value of the Datasets row is 0.09434, greater than $\alpha = 0.05$. Thus, it fails to reject the first null hypothesis. This means that the means of RMSE on the data sets are the same. On the Models row, P-value is 0.00001, much lower than the value of α. It means that the second null hypothesis is rejected. Hence, the means of RMSE obtained by selected models are different. However, doing the post-hoc test among the pairs of five of these models shows that the differences are insignificant.

R^2: For R^2 values, two null hypotheses in this analysis are the same as RMSE. Two-way ANOVA without replication is also performed, and the results are given in Table 13. As shown in Table 13, the values of the P-value in the two first rows are 0.0216 and 0.0215, respectively. These values are both lower than the α value (0.05). Thus, two null hypotheses

TABLE 14. ANOVA analysis for values of time-consuming.

Source of Variation	SS	df	MS	F	P-Value	F crit
Datasets	0.002	2	0.0011	6.439	0.0216	4.459
Models	0.004	4	0.0009	5.343	0.0215	3.838
Error	0.001	8	0.0002			
Total	0.007	14				

are rejected. This leads to the differences of means of R^2 on data sets and the models as well. To compare the means of R^2 obtained by CO-SPATIAL CFIS+ and our proposed method, a post-hoc (Bonferroni) test is done. The results show the difference of means of R^2 obtained by the proposed method and that of CO-SPATIAL CFIS+.

Time Consuming: Two-way ANOVA without replication is applied with the two null hypotheses mentioned above to analyze the runtime of five models on different data sets. The results of this analysis are shown in Table 14.

As same as the values of P-value in Table 12, the values in Table 14 show that the means of time-consuming on data sets are no different (P-value is 0.94761, greater than alpha). However, the means of time-consuming on models are different (P-value is 000002, lower than α). The post-hoc tests show significant differences between our method and others. Based on the comparison in Figure 16, the proposed method takes the lowest run time among the five models.

VI. CONCLUSION

This study presented a novel spatial inference system capable of adapting to new data. Our proposed model generates a rulebase directly from the image and trains the parameters in the rule system based on the Co-Spatial-CFIS+ model. This new rulebase and the previous Co-Spatial-CFIS+ rulebase are evaluated using a complex fuzzy measure. This measure is built by determining the intersection domain between two rule spaces; Then, it is used to estimate the removal, merging, or addition of a new rule into the current rulebase, resulting in a more suitable set of rules for image prediction. To demonstrate the effectiveness of the proposed approach, the model was applied to the SCI dataset of the U.S. Navy and compared to state-of-the-art studies in detecting RSI changes.

Despite the initial positive results, the model has some limitations. Determining the intersection domain of rules and summarizing rules is quite simple, directly affecting the model results. In addition, although the model gives better results than other methods on the same platform, determining the solution space is still simple, using only the Gaussian function. This limitation is also the primary motivation for the team to research and develop in the future. That is to give way to determine the regions of the solution space and synthesize the rules to improve the performance and the time in the forecasting process.

APPENDIX

Source codes and Dataset of this paper are available at the following address: https://github.com/vietdslab/SpatialCFIS-

REFERENCES

[1] O. Ghorbanzadeh, H. Rostamzadeh, T. Blaschke, K. Gholaminia, and J. Aryal, "A new GIS-based data mining technique using an adaptive neuro-fuzzy inference system (ANFIS) and k-fold cross-validation approach for land subsidence susceptibility mapping," *Natural Hazards*, vol. 94, no. 2, pp. 497–517, Nov. 2018.

[2] G. Castellano, C. Castiello, A. Montemurro, G. Vessio, and G. Zaza, "Segmentation of remotely sensed images with a neuro-fuzzy inference system," in *Proc. WILF*, 2021, pp. 1–9.

[3] I. Ali, F. Cawkwell, E. Dwyer, and S. Green, "Modeling managed grassland biomass estimation by using multitemporal remote sensingdata— A machine learning approach," *IEEE J. Sel. Topics Appl. Earth Observ. Remote Sens.*, vol. 10, no. 7, pp. 3254–3264, Jul. 2017.

[4] Y. Yin, Y. Sheng, and J. Qin, "Interval type-2 fuzzy C-means forecasting model for fuzzy time series," *Appl. Soft Comput.*, vol. 129, Nov. 2022, Art. no. 109574.

[5] D.-H. Pham, C.-M. Lin, V. Nam Giap, T.-T. Huynh, and H.-Y. Cho, "Wavelet interval type-2 Takagi–Kang–Sugeno hybrid controller for time-series prediction and chaotic synchronization," *IEEE Access*, vol. 10, pp. 104313–104327, 2022.

[6] X. Xie, C. Wei, Z. Gu, and K. Shi, "Relaxed resilient fuzzy stabilization of discrete-time Takagi–Sugeno systems via a higher order time-variant balanced matrix method," *IEEE Trans. Fuzzy Syst.*, vol. 30, no. 11, pp. 5044–5050, Nov. 2022.

[7] H. Liang, L. Chen, Y. Pan, and H.-K. Lam, "Fuzzy-based robust precision consensus tracking for uncertain networked systems with cooperative— Antagonistic interactions," *IEEE Trans. Fuzzy Syst.*, vol. 31, no. 4, pp. 1362–1376, Apr. 2023.

[8] L. An and G.-H. Yang, "Distributed secure state estimation for cyber–physical systems under sensor attacks," *Automatica*, vol. 107, pp. 526–538, Sep. 2019.

[9] L. Ke, Y. Lin, Z. Zeng, L. Zhang, and L. Meng, "Adaptive change detection with significance test," *IEEE Access*, vol. 6, pp. 27442–27450, 2018.

[10] V. Ferraris, N. Dobigeon, Q. Wei, and M. Chabert, "Detecting changes between optical images of different spatial and spectral resolutions: A fusion-based approach," *IEEE Trans. Geosci. Remote Sens.*, vol. 56, no. 3, pp. 1566–1578, Mar. 2018.

[11] L. Zhang and G.-H. Yang, "Observer-based adaptive decentralized fault-tolerant control of nonlinear large-scale systems with sensor and actuator faults," *IEEE Trans. Ind. Electron.*, vol. 66, no. 10, pp. 8019–8029, Oct. 2019.

[12] T. T. Ngan, L. T. H. Lan, M. Ali, D. Tamir, L. H. Son, T. M. Tuan, N. Rishe, and A. Kandel, "Logic connectives of complex fuzzy sets," *Romanian J. Inf. Sci. Technol.*, vol. 21, 344–358, Jan. 2018.

[13] M. Ali and F. Smarandache, "Complex neutrosophic set," *Neural Comput. Appl.*, vol. 28, no. 7, pp. 1817–1834, Jul. 2017.

[14] M. Ali, L. Q. Dat, L. H. Son, and F. Smarandache, "Interval complex neutrosophic set: Formulation and applications in decision-making," *Int. J. Fuzzy Syst.*, vol. 20, no. 3, pp. 986–999, Mar. 2018.

[15] S. Greenfield, F. Chiclana, and S. Dick, "Interval-valued complex fuzzy logic," in *Proc. IEEE Int. Conf. Fuzzy Syst. (FUZZ-IEEE)*, Jul. 2016, pp. 2014–2019.

[16] H. Garg and D. Rani, "Some generalized complex intuitionistic fuzzy aggregation operators and their application to multicriteria decision-making process," *Arabian J. Sci. Eng.*, vol. 44, no. 3, pp. 2679–2698, Mar. 2019.

[17] G. Selvachandran, S. G. Quek, L. T. H. Lan, L. H. Son, N. L. Giang, W. Ding, M. Abdel-Basset, and V. H. C. de Albuquerque, "A new design of Mamdani complex fuzzy inference system for multiattribute decision making problems," *IEEE Trans. Fuzzy Syst.*, vol. 29, no. 4, pp. 716–730, Apr. 2021.

[18] C. H. Tu and C. Li, "Multiple function approximation—A new approach using complex fuzzy inference system," in *Proc. Asian Conf. Intell. Inf. Database Syst.* Cham, Switzerland: Springer, 2018, pp. 243–254.

[19] K. Subramanian, R. Savitha, and S. Suresh, "A complex-valued neuro-fuzzy inference system and its learning mechanism," *Neurocomputing*, vol. 123, pp. 110–120, Jan. 2014.

[20] C.-H. Tu and C. Li, "Multiple function approximation—A new approach using asymmetric complex fuzzy inference system," *Vietnam J. Comput. Sci.*, vol. 6, no. 4, pp. 407–422, Nov. 2019.

[21] Y. Liu and F. Liu, "An adaptive neuro-complex-fuzzy-inferential modeling mechanism for generating higher-order TSK models," *Neurocomputing*, vol. 365, pp. 94–101, Nov. 2019.

[22] Z. Chen, S. Aghakhani, J. Man, and S. Dick, "ANCFIS: A neurofuzzy architecture employing complex fuzzy sets," *IEEE Trans. Fuzzy Syst.*, vol. 19, no. 2, pp. 305–322, Apr. 2011.

[23] O. Yazdanbakhsh and S. Dick, "Multi-variate timeseries forecasting using complex fuzzy logic," in *Proc. Annu. Conf. North Amer. Fuzzy Inf. Process. Soc. (NAFIPS), 5th World Conf. Soft Comput. (WConSC)*. IEEE, Aug. 2015, pp. 1–6.

[24] O. Yazdanbakhsh and S. Dick, "FANCFIS: Fast adaptive neuro-complex fuzzy inference system," *Int. J. Approx. Reasoning*, vol. 105, pp. 417–430, Feb. 2019.

[25] T. M. Tuan, L. T. H. Lan, S.-Y. Chou, T. T. Ngan, L. H. Son, N. L. Giang, and M. Ali, "M-CFIS-R: Mamdani complex fuzzy inference system with rule reduction using complex fuzzy measures in granular computing," *Mathematics*, vol. 8, no. 5, p. 707, May 2020.

[26] L. T. H. Lan, T. M. Tuan, T. T. Ngan, L. H. Son, N. L. Giang, V. T. N. Ngoc, and P. Van Hai, "A new complex fuzzy inference system with fuzzy knowledge graph and extensions in decision making," *IEEE Access*, vol. 8, pp. 164899–164921, 2020.

[27] L. T. Giang, L. H. Son, N. L. Giang, T. M. Tuan, N. V. Luong, M. D. Sinh, G. Selvachandran, and V. C. Gerogiannis, "A new co-learning method in spatial complex fuzzy inference systems for change detection from satellite images," *Neural Comput. Appl.*, vol. 35, pp. 4519–4548, Oct. 2022.

[28] K. Mondal, P. Dutta, and S. Bhattacharyya, "Feature based fuzzy rule base design for image extraction," 2012, *arXiv:1206.3633*.

[29] A. Zaher, Y. N'goran, F. Thiery, S. Grieu, and A. Traoré, "Fuzzy rule-based model for optimum orientation of solar panels using satellite image processing," *J. Phys., Conf. Ser.*, vol. 783, Jan. 2017, Art. no. 012058.

[30] A. Senthilselvi, J. S. Duela, R. Prabavathi, and D. Sara, "Performance evaluation of adaptive neuro fuzzy system (ANFIS) over fuzzy inference system (FIS) with optimization algorithm in de-noising of images from salt and pepper noise," *J. Ambient Intell. Humanized Comput.*, pp. 1–6, Mar. 2021.

[31] L. Tang, D. Wu, H. Wang, M. Chen, and J. Xie, "An adaptive fuzzy inference approach for color image steganography," *Soft Comput.*, vol. 25, no. 16, pp. 10987–11004, Aug. 2021.

[32] B. SziovCá, S. Nagy, and L. T. Kóczy, "The effects of preprocessing on colorectal polyp detecting by fuzzy algorithm," in *Recent Developments and the New Direction in Soft-Computing Foundations and Applications*. Cham, Switzerland: Springer, 2021, pp. 347–357.

[33] L.-C. Duţu, G. Mauris, and P. Bolon, "A fast and accurate rule-base generation method for Mamdani fuzzy systems," *IEEE Trans. Fuzzy Syst.*, vol. 26, no. 2, pp. 715–733, Apr. 2018.

[34] D. Ramot, R. Milo, M. Friedman, and A. Kandel, "Complex fuzzy sets," *IEEE Trans. Fuzzy Syst.*, vol. 10, no. 2, pp. 171–186, Aug. 2002.

[35] A. Borji and M. Hamidi, "Evolving a fuzzy rule-base for image segmentation," *Int. J. Intell. Technol.*, vol. 2, pp. 471–476, Jul. 2007.

[36] V. Kreinovich, C. Quintana, and L. Reznik, "Gaussian membership functions are most adequate in representing uncertainty in measurements," in *Proc. NAFIPS*, vol. 92, Dec. 1992, pp. 15–17.

[37] R. A. Hummel, "Histogram modification techniques," *Comput. Graph. Image Process.*, vol. 4, no. 3, pp. 209–224, Sep. 1975.

[38] M. S. Bajwa, A. P. Agarwal, and S. Manchanda, "Ternary search algorithm: Improvement of binary search," in *Proc. 2nd Int. Conf. Comput. Sustain. Global Develop. (INDIACom)*, Mar. 2015, pp. 1723–1725.

[39] National Oceanic and Atmospheric Administration. *MTSAT West Color Infrared Loop*. Accessed: Aug. 1, 2021. [Online]. Available: https://www.star.nesdis.noaa.gov/GOES/index.php

[40] Z. Shen, Y. Zhang, J. Lu, J. Xu, and G. Xiao, "SeriesNet: A generative time series forecasting model," in *Proc. Int. Joint Conf. Neural Netw. (IJCNN)*, Jul. 2018, pp. 1–8, doi: 10.1109/IJCNN.2018.8489522.

[41] B. Du, L. Ru, C. Wu, and L. Zhang, "Unsupervised deep slow feature analysis for change detection in multi-temporal remote sensing images," *IEEE Trans. Geosci. Remote Sens.*, vol. 57, no. 12, pp. 9976–9992, Dec. 2019.

[42] L. H. Son and P. H. Thong, "Some novel hybrid forecast methods based on picture fuzzy clustering for weather nowcasting from satellite image sequences," *Int. J. Speech Technol.*, vol. 46, no. 1, pp. 1–15, Jan. 2017.

[43] K. Mondal, P. Dutta, and S. Bhattercharyya, "Gray image extraction using fuzzy logic," in *Proc. 2nd Int. Conf. Adv. Comput. Commun. Technol.*, Jan. 2012, pp. 289–296.

LE TRUONG GIANG received the engineering degree in computer science and the master's degree in computer science from the Thai Nguyen University of Information and Communication Technology (ICTU), in 2011 and 2014, respectively. He is currently pursuing the Ph.D. degree with the Institute of Information Technology (IoIT), Vietnam Academy of Science and Technology, Hanoi, Vietnam. He is with the Quality Assurance Center, Hanoi University of Industry. His research interests include optimization, machine learning, data mining, artificial intelligence, soft computing, and fuzzy computing.

LE HOANG SON received the Ph.D. degree in mathematics and informatics from the VNU University of Science, Vietnam National University (VNU), in conjunction with Politecnico di Milano, Italy, in 2013.

He has been promoted to Associate Professor of information technology in Vietnam, since 2017. He was a Senior Researcher and the Vice Director of the Center for High-Performance Computing, VNU University of Science, VNU, from 2007 to 2018. Since August 2018, he has been a Senior Researcher with the Department of Multimedia and Virtual Reality, VNU Information Technology Institute. His major research interests include artificial intelligence, data mining, soft computing, fuzzy computing, fuzzy recommender systems, and geographic information systems.

Dr. Hoang Son is a member of the Vietnam Journalists Association, the International Association of Computer Science and Information Technology, the Vietnam Society for Applications of Mathematics, and the Key Laboratory of Geotechnical Engineering and Artificial Intelligence, University of Transport Technology. He is an Associate Editor of the *Journal of Intelligent and Fuzzy Systems* (SCIE), IEEE Access (SCIE), *Data Technologies and Applications* (SCIE), *International Journal of Data Warehousing and Mining* (SCIE), *Neutrosophic Sets and Systems* (ESCI), *Vietnam Research and Development on Information and Communication Technology*, *VNU Journal of Science: Computer Science and Communication Engineering*, and *Frontiers in Artificial Intelligence*. He is the Guest Editor of several Special Issues with the *International Journal of Uncertainty, Fuzziness and Knowledge-Based Systems* (SCIE), and *Journal of Ambient Intelligence and Humanized Computing*. He serves on the editorial board for *Applied Soft Computing* (SCIE), *PLOS One* (SCIE), *International Journal of Web and Grid Services* (SCIE), *International Journal of Ambient Computing and Intelligence* (ESCI), and *Vietnam Journal of Computer Science and Cybernetics*.

NGUYEN LONG GIANG received the Ph.D. degree in mathematics from the Institute of Information Technology (IoIT), Vietnam Academy of Science and Technology, in 2012. He is currently an Associate Professor with IoIT, Vietnam Academy of Science and Technology. His research interests include artificial intelligence, data mining, soft computing, and fuzzy computing. He serves as an Editorial Board Member for the *Vietnam Journal of Computer Science and Cybernetics* (JCC). He has served as the TPC Chair for some international conferences, such as IJCRS 2019, AICI 2019, MARR 2019, IEEE-RIVF 2019, SoICT 2019, and KSE 2017.

NGUYEN VAN LUONG received the degree in information technology from the Hanoi University of Industry, in 2020, and the master's degree from the Institute of Information Technology (IoIT), Vietnam Academy of Science and Technology. He is currently with the Quality Assurance Center, Hanoi University of Industry. His research interests include image processing, machine learning, and soft computing.

TRAN MANH TUAN received the bachelor's degree in applied mathematics and informatics from the Hanoi University of Science and Technology, in 2003, the master's degree in computer science from Thai Nguyen University, in 2007, and the Ph.D. degree, in July 2017. He is currently a Lecturer with the Faculty of Computer Science and Engineering, Thuyloi University. His research interests include artificial intelligence, data mining, soft computing, and fuzzy computing.

LUONG THI HONG LAN received the degree from the Hanoi University of Technology, in 2002, and the Ph.D. degree in computer science from the Institute of Information Technology (IoIT), Vietnam Academy of Science and Technology, Hanoi, Vietnam, in 2021. She is currently with the Faculty of Computer Science and Engineering, Thuyloi University. Her research interests include artificial intelligence, data mining, soft computing, and fuzzy computing.

NGUYEN TRUONG THANG received the Ph.D. degree from the Japan Advanced Institute of Science and Technology (JAIST), Japan, in 2005. He is currently with the Institute of Information Technology (IoIT), Vietnam Academy of Science and Technology. His major research interests include software quality assurance, software verification, program analysis, data mining, and machine learning.

• • •